# Water Resources Research

### RESEARCH ARTICLE

10.1029/2022WR032544

#### **Key Points:**

- · Estuarine response to SLR is found non-linear and influenced by both hydrodynamics and morphological evolution
- Erosion in the middle of estuary favors a concave shaped water level difference and increase water level slope at upstream
- Under severe SLR case, increased water surface slope and weakened upstream deposition together decrease riverine flood risk in the upstream

#### Correspondence to:

W. Ni. wumingni@zju.edu.cn

#### Citation:

Ni, W., Morgan, J. A., Horner-Devine, A. R., Kumar, N., & Ahrendt, S. (2022). Impacts of sea-level rise on morphodynamics and riverine flooding in an idealized estuary. Water Resources Research, 58, e2022WR032544. https:// doi.org/10.1029/2022WR032544

Received 8 APR 2022 Accepted 9 DEC 2022

#### **Author Contributions:**

Formal analysis: Wuming Ni Investigation: Wuming Ni Project Administration: Alexander R. Horner-Devine

Software: Wuming Ni, Jacob A. Morgan, Nirnimesh Kumar

Supervision: Alexander R. Horner-Devine

Writing - original draft: Wuming Ni Writing - review & editing: Wuming Ni, Jacob A. Morgan, Alexander R. Horner-Devine, Shelby Ahrendt

© 2022. American Geophysical Union. All Rights Reserved.

# Impacts of Sea-Level Rise on Morphodynamics and Riverine Flooding in an Idealized Estuary

Wuming Ni<sup>1</sup>, Jacob A. Morgan<sup>2,3</sup>, Alexander R. Horner-Devine<sup>2</sup>, Nirnimesh Kumar<sup>2</sup>, and Shelby Ahrendt<sup>2</sup>

<sup>1</sup>Department of Civil Engineering, Zhejiang University, Hangzhou, China, <sup>2</sup>Department of Civil and Environmental Engineering, University of Washington, Seattle, WA, USA, 3Now at Paradigm Environmental, Nashville, TN, USA

**Abstract** This research simulates the morphodynamic evolution of an idealize estuary under four different SLR scenarios of increasing severity to investigate how SLR will influence riverine flooding in estuaries. We find that estuarine response to SLR is influenced by both morphological changes to channel capacity and the associated changes to channel hydrodynamics. Low and moderate SLR scenarios result in an increase in flood extent throughout the estuary relative to the no SLR base case. Surprisingly, more severe SLR scenarios result in decreased flood extent in upstream reaches. This shift is due to penetration of tidal energy and erosion further upstream with greater SLR, which increases channel capacity locally. A periodic pattern of local sediment transport is additionally observed due to SLR, which we attribute to the time response lag between hydrological and morphological response. The finding that increased SLR does not result in increased flood extent everywhere emphasizes that flood mitigation measures need to carefully account for non-linear responses in the estuarine morphodynamic systems, such as the feedbacks resulting from increased tidal erosion.

# 1. Introduction

Sea-level rise in response to global climate change is becoming an increasingly important factor in disaster prevention in estuaries. SLR has been accelerating worldwide throughout the twentieth century and based on satellite data the trend will continue in the future (Le Bars et al., 2017). Estuaries are key areas that transport water and sediment, accommodate coastal communities, and provide habitat for animal species. They are susceptible to flooding from both storm surge inundation and riverine flooding. Generally, higher sea levels are expected to inundate further inland and increase the frequency and severity of coastal flooding associated with high tide, storm surge, and episodic flooding associated with waves (Hamman, 2012; Hamman et al., 2016).

Riverine flooding occurs when the volume of water in a waterway exceeds the channel conveyance capacity. While changes in flood frequency have traditionally been related to trends in precipitation or discharge, incidents like the flood in Pacific, WA, along with a number of field and experimental studies, demonstrate that reduction of channel conveyance caused by sediment deposition (aggradation) can lead to more frequent floods and amplify flood hazards (Ahrendt et al., 2022; Lane & Thorne, 2007; Lane et al., 2007; Slater et al., 2015; Stover & Montgomery, 2001).

SLR can raise mean water level along the channel and modify tidal range (Khojasteh et al., 2019; Passeri et al., 2016), subjecting large areas of low-lying floodplains in the lower reaches to increased flood extent. SLR also forces tides further upstream, shapes estuarine tidal asymmetry, and increases salinity intrusion (Hong et al., 2020; Mulamba et al., 2019; Vu et al., 2018). Changes in the hydrodynamic regime including residual current velocity, tidal current velocity and, tidal asymmetry are influenced by the estuarine shape and external forces, affect the tidal residual sediment transport and shaped the long-term estuarine morphodynamic (Khojasteh, Glamore, et al., 2021). Both analytical and numerical methods have been applied to investigate the effect on SLR on estuarine hydrodynamic and morphodynamic in the last few decades. Analytical approaches have been applied to predict estuarine hydrodynamics for certain simplified types of estuaries, like (Cai et al., 2014; Prandle, 2009; Van Rijn, 2011). For most analytical studies of alluvial estuaries, the estuarine bathymetry is simplified and its shape is fixed to an exponentially varying width and depth, making it difficult to reveal the morphological response of estuary to external forcings in detail.

Numerical modeling of estuaries can consider various types of estuary and different driving forces compared with analytical methods. Thus far, most numerical studies have focused on the offshore or intertidal area (Bilskie

NI ET AL. 1 of 17 et al., 2014; Elmilady et al., 2020; Gutierrez et al., 2011), while limited attention was paid to morphodynamic evolution in upstream reaches. Furthermore, most hydrodynamic studies apply a simplified 1-D model to minimize computation (e.g., Canestrelli et al., 2014; Yuan et al., 2020).

In this paper, a process-based 3-D morphodynamic model of an idealized estuary is employed to investigate the effects of SLR on long-term morphodynamic change and riverine flood extent. Specifically, we address the following question: how does the morphodynamic response to SLR in an estuary influence the extent of flooding associated with a high river discharge flood event.

We first describe the model setup and validation in Sections 2 and 3, respectively. Then we examine how flood extent and factors associated with flood extent evolve under different SLR scenarios in Section 4. The hydrodynamic and morphodynamic adjustment under SLR influence is presented in Section 5 and their effect on tidal residual sediment transport is presented in Section 6. Morphological and hydrological response of estuary to SLR is examined in Section 7. Finally, we discuss the application of results in this research in real estuaries in Section 8.

# 2. Model Setup

We developed a simplified idealized model based on the Skagit River in Washington State, US using Delft3D software which solves the depth-averaged unsteady shallow-water equations across a boundary fitted grid (Lesser et al., 2004). The Skagit River is the largest river draining into Puget Sound, Washington with respect to water discharge and sediment delivery. It is responsible for about 35% of all fluvial discharge and 43% of all fluvial sediment delivery into Puget Sound, and influences flood hazards in its lowland (Czuba et al., 2011). The model domain is a 30 km by 15 km rectangle of which 10 by 15 km is the coastal ocean (Figure 1a). The upstream boundary is located 20 km from the estuary mouth, similar to the location of the town of Mt. Vernon, WA. Mt. Vernon has been chosen as the upstream boundary for several numerical studies focusing on the tide and sediment transport in Skagit Bay area (e.g., Yang & Khangaonkar 2009). Tidal influence is minor beyond this point. In our simulations, no tidal signal is present at cells near the upstream boundary.

Boundary conditions are chosen based on historical records of the Skagit River in the last few decades by Curran et al. (2016). The river discharge at Mt. Vernon is regulated by upstream mainstem dams with an annual mean flow of  $468 \text{ m}^3$ /s and an annual sediment load of  $2.8 \times 10^6 \text{ ton/yr}$ . The suspended sediment load mainly consists of fine sediment (silt- and clay-sized particles smaller than 0.0625 mm) and bedload mainly consists of medium-sized sand (0.25-0.5 mm). The Skagit River empties into Skagit Bay, which is mesotidal and primarily dominated by semi-diurnal tides. Based upon these river characteristics, a constant riverine water discharge of  $400 \text{ m}^3$ /s is applied at the model upstream boundary. The sediment flux supplied from the upstream boundary varies for different model stages and will be introduced in detail later in this section. At the offshore boundary, a symmetric semi-diurnal tide (M2 tide) with a tidal range of 4 m and an equilibrium sediment concentration boundary are imposed. At the two lateral coastal ocean boundaries, a zero-gradient Neumann boundary is applied. It should be noted that coastal flooding like storm surge is not included in this study as we focus on riverine flooding.

The grid resolution is 50 and 100 m in the cross-channel and along-channel directions, respectively, with five equally spaced sigma layers in the vertical. The time step is set to 0.25 min. For bank erosion, a dry cell erosion parameter (ThetSD) of 0.5 is applied. To reduce computational time and costs, the morphodynamic acceleration factor (MorFac) of 1,000 is used for the long term morphodynamic runs described below. This technique has been widely applied in simulations of the long-term morphodynamic evolution of estuaries (Guo et al., 2014; Morgan et al., 2020; Roelvink, 2006). Following Curran et al. (2016), a medium sand grain size of 0.5 mm and a mud erosion parameter of  $1.0 \cdot 10^{-4} \, \text{kg} \cdot \text{m}^2 \cdot \text{s}$  is used. The Engelund and Hansen (1967) transport formula is chosen for the sand flux calculation:

$$q_s = \frac{0.05u^5}{\sqrt{g}C^3(s-1)^2d} \tag{1}$$

in which, u represents the longitudinal flow velocity; g is the gravitational acceleration; C and s are the Chezy roughness coefficient and density ratio respectively; and d is the sediment grain size. For simplification, a constant C value of 65 m<sup>1/2</sup> s<sup>-1</sup> is used following Guo et al. (2014). For the mud transport calculation, the flux between

NI ET AL. 2 of 17

Water Resources Research

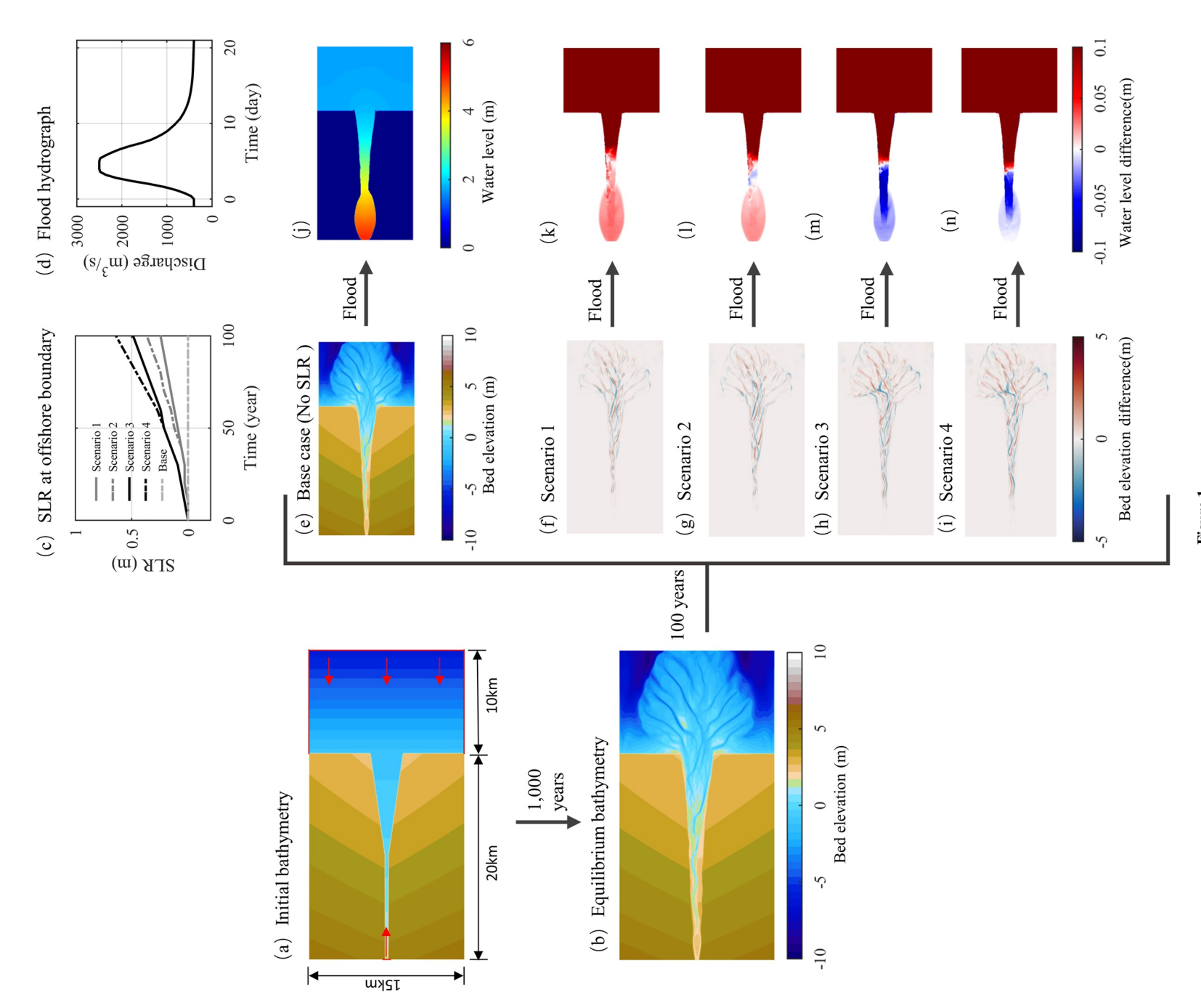


Figure 1.

3 of 17NI ET AL.

# Water Resources Research

Table 1 Model Parameter Settings Applied in Numerical Simulations Based on the Delft3D Software	
Property	Parameter
Domain size	$(20 + 10) \cdot 15 \text{ km}^2$
Cell size	50 – 100 m
Sand diameter	0.5 mm
Mud erosion parameter	$1.0\cdot 10^{-4}kg\cdot m^2\cdot s$
Chezy roughness	$65 \text{ m}^{1/2} \cdot \text{s}^{-1}$
Morphodynamic acceleration factor (MorFac)	1,000
Threshold depth for dry cell checking	$1\cdot 10^{-4}\mathrm{m}$
Dry cell erosion parameter	0.5
Threshold sediment thickness for transport	0.05 m
Bed slope effect on bedload transport	3 (Koch & Flokstra formulation)
	(Ashld = 0.2, Bshld = 0.5)
Spin-up interval of morphological change	1,440 min

water flow and bed was calculated with the Partheniades-Krone formulations (Partheniades, 1965). Other model parameters are summarized in Table 1. Cells where water depth is below 0.1 mm are considered dry. When local sediment thickness is lower than 0.05 m, the sediment transport is reduced (though this does not happen because the initial bed thickness is 50 m). Dry cell erosion is responsible for bank erosion here and a default value of 0.5 is applied. The Koch and Flokstra (1980) formulation is used to account for the influence of bed level gradients on bedload transport.

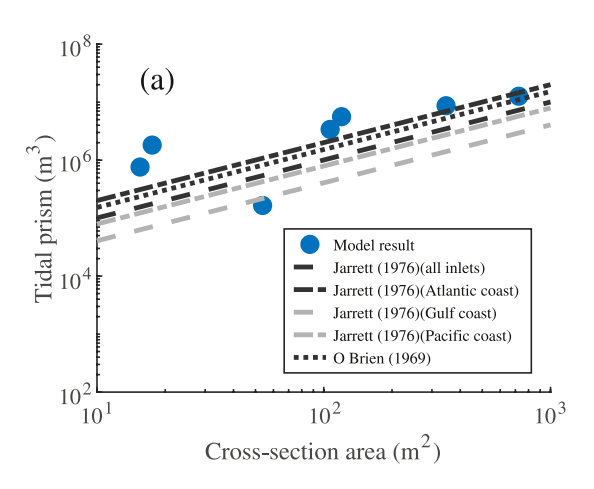
The simulations follow three stages as shown in Figure 1:

- 1. 1000-Year Model: We generate an equilibrium bathymetry (Figure 1b) by running a 1000-year morphodynamic simulation with equilibrium sediment concentration supplied to the upstream boundary. The initial bathymetry (Figure 1a) consists of a 600 m-wide straight river connected to the ocean by a funnel-shaped estuary with a maximum width of 3 km at the mouth. The channel bottom elevation decreases exponentially from 1.5 m at the upstream boundary to -2 m at the estuary mouth. In order to simulate bank erosion and flood inundation processes, we include a lateral floodplain in our simulations which decreases in elevation exponentially from 5 to 2 m in the along-channel direction and has a constant slope of 0.0002 in the cross-channel direction. Offshore, the bottom elevation decreases with a constant slope of 0.0005 in the along-channel direction.
- 2. 100-Year Model: Five different 100-year SLR scenarios are simulated (including a base model with no SLR, Figure 1c) using sea-level values projected by Miller et al. (2018). These scenarios consist of a no-SLR case and four SLR cases representing different representative concentration pathways (RCP 4.5 and 8.5) and different likelihoods (50% and 90%). A constant sediment flux of  $3 \cdot 10^{-3}$  m³/s and an identical concentration of mud flux are applied at the upstream boundary. These simulations are referred to as the base model and scenarios 1–4 from the mildest to the most severe SLR conditions.
- 3. Flood Model: In order to evaluate the change in flood vulnerability in the estuary, a design flood hydrograph (Figure 1d) is applied to the upstream boundary using the morphology extracted from each SLR scenario. The same hydrograph is tested for the modeled bathymetry every 20 years to evaluate the evolution of flood extent. The hydrograph is modified from a 2006 flood event in the Skagit river using a dimensionless unit hydrograph (Mockus, 1957). The hydrograph has a length of 21 days, a base discharge of 400 m³/s, which is consistent with previous morphodynamic models, and a peak discharge of 2500 m³/s.

**Figure 1.** Schematic diagram of simulation steps. (a): Initial bathymetry, red lines represent open boundary, arrows represent external forcing including river discharge and tidal components; (b): Equilibrium bathymetry after 1,000 years of morphological evolution under equilibrium sediment concentration supplied from upstream; (c): SLR value projected by Miller et al. (2018), applied at offshore boundary for each case; (d): Design hydrograph for flood test; (e): Morphology of base model under no SLR conditions after 100 years of morphological evolution; (f, g, h, i): Bed level difference compared with base model for each scenario, red indicates bed aggradation and blue indicates erosion; (j): Water level during peak discharge for flood test with morphology from base model at the 100th year; (k, l, m, n): Water level difference compared with no SLR condition for each scenario using morphology at the 100th year.

NI ET AL. 4 of 17

19447973, 2022, 12, Downloaded from https://agupubs.onlinelibrary.wiley.com/doi/10.1029/2022WR032544 by University Of Washington Lib S, Wiley Online I



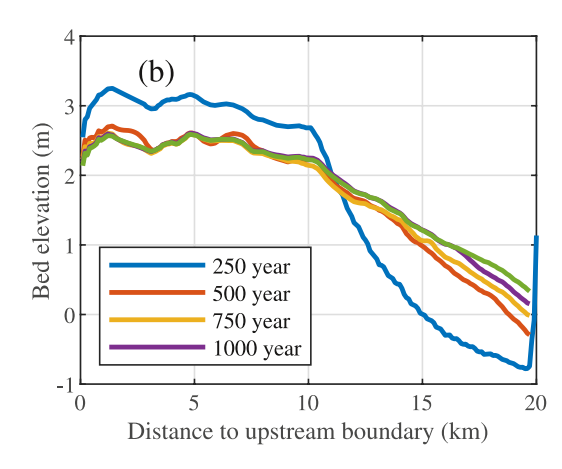


Figure 2. (a) Tidal prism and characteristic cross-sectional area relationship comparison with prior study, Tidal prism represents the water volume flow through typical cross-section during ebb tide, and characteristic cross-sectional area was calculated as the channel area below mean sea-level; (b) Cross-channel averaged bed level evolution during the 1000-year equilibrium simulation.

#### 3. Model Validation

Idealized models have been widely used to explain long-term morphodynamics in estuaries (Braat et al., 2017; Lanzoni & Seminara, 2002; Olabarrieta et al., 2018; Yu et al., 2012). Here we consider a simplified idealized estuary aiming to focus on the main processes that affect local morphological evolution and flood extent: riverine discharge, tidal current and tidal asymmetry induced by overtides. Due to limited access to field data for the idealized model, model validation was conducted based on observations on model morphological evolution and comparison with geomorphic relationship found in prior studies.

An equilibrium bed profile is expected to be reached on centennial to millennial time scales for an idealized model with stable boundary conditions. The equilibrium condition is characterized by a uniform residual sediment transport flux, a vanishing bed elevation change, and a developing trend toward the empirical relationship between ebb tidal volume and cross-sectional area below mean sea-level (Guo et al., 2014; Moore et al., 2009). The empirical equilibrium PA relationship between tidal prism and channel cross-sectional area suggests that characteristic cross-sectional area is exponentially related to tidal prism (van der Wegen et al., 2010). Attempts have been made to physically explain the PA relationship based on the concept of critical shear stress and the equilibrium sediment concentration, which all point to a dynamic equilibrium in tidal inlets. Figure 2a compares tidal prism and characteristic channel area in our model with several empirical relationships. They match well and follow a consistent trend with the exception of one model data point, which falls below the trend and represents the upstream-most cross-section plotted. While the other model data points are for the multi-thread lower estuary, the anomalous point corresponds to a cross-section with a deep, single-thread channel. Figure 2b shows the cross-channel averaged bed elevation evolution through 1,000 years. Bed level change for the upper-most 16 km is on the scale of centimeters in the last 250 years, indicating that the morphology has reached a steady state equilibrium.

# 4. Flood Extent Under SLR Influence

The main objective of our work is to understand how morphological changes resulting from SLR may influence riverine flooding in the future. Here, we focus our area of interest within the estuary rather than the offshore area. Figure 3 shows the water level difference between base model and each scenario case during the peak discharge period of the design flood. All SLR scenarios result in morphodynamic changes that alter inundation magnitude relative to the base scenario. As sea-level increases in scenarios 1 and 2, we observe consistent increasing flood extent, while for scenarios 3 and 4, riverine flood extent peaks in the 60th year (Figures 3m and 3r) and then decreases (Figures 3o and 3t). Also, we see a consistent decrease in flood extent in the middle reach of the estuary (~7–10 km) beginning at the 60th year for all scenarios (Figures 3c, 3h, 3m, and 3r). Surprisingly, the greatest SLR scenarios do not result in the greatest flood extent upstream (Figure 4). Scenario 1 experiences the most

NI ET AL. 5 of 17

19447973, 2022, 12, Downloaded from https://agupubs.onlinelibrary.wiley.com/ab/10.1029/2022WR032544 by University Of Washington Lib S, Wiley Online Library on [09.01/2023]. See

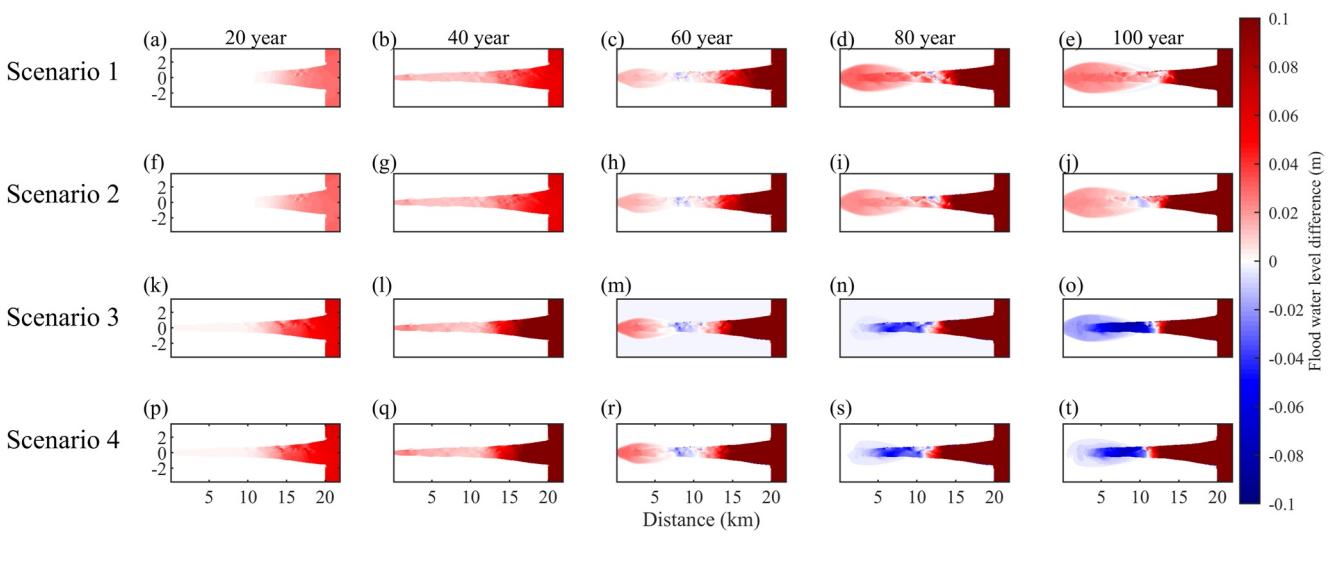


Figure 3. Difference in maximum water-level during peak discharge of the design flood compared with base model (m). Morphology under different SLR conditions every 20 years is tested. Results are compared with flood test results using morphology from base model at the same timing. Color red represents flood extent increase; blue represents decrease.

severe riverine flooding while scenario 3 experiences the mildest, and scenario 4 which has the highest SLR sits between scenario 3 and the base model. This indicates that riverine extent does not simply increase with SLR.

Flood extent change can be associated with many factors including changes in bed elevation, bed roughness, channel width, and water slope. Based on the classic Chezy's formula (Sturm, 2001), water depth can be expressed as a function of discharge, water surface slope, and flow resistance. To investigate the sensitivity of estuarine flood extent change caused by SLR during the peak discharge of the flood tests, the water level in the base model and the four SLR scenarios is calculated as:

$$H = \left(\frac{Q}{W \cdot C \cdot S^{1/2}}\right)^{2/3} + B \tag{2}$$

in which H is water level; Q is river discharge; W is channel width; C represents Chezy's roughness; S represents water surface slope; and B represents bed elevation. It should be noted that hydraulic radius is replaced by water

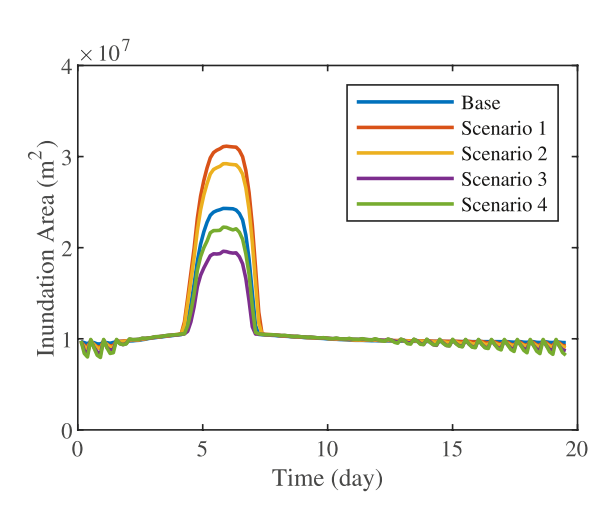


**Figure 4.** Flood inundation area during flood test for base model and all four scenarios using the morphology at the end of the 100-year SLR simulations. Cells with a water depth larger than 0.01 m are considered inundated.

depth here since the width to depth ratio is very large. For each scenario, Equation 2 gives us a prediction of the water surface elevation H in terms of the values of H, W, C, S and B determined for each 1 km section of the estuary from the model output. In Figure 5 the difference between the surface elevation from the model during peak flood discharge in scenarios 1–4 and the base case is compared to the difference predicted using Equation 2. The Chezy equation (Equation 2) provides a good prediction of the water surface elevation differences, showing that it captures the dynamics that determine the water surface elevation.

We also use the Chezy equation to determine the relative contributions of width, roughness, surface slope and bed elevation to the total water level change during the peak discharge period of flood tests. Each contribution is calculated based on the difference in water level by changing one factor at a time while holding others fixed using Equation 2. The predictions based on Equation 2 (green line with circles) are consistent with model results (gray dashed line), indicating that our errors in calculating different physical parameters are minor. For example, to compute the contribution to water level associated with bottom roughness for scenario 1 (Figure 5a, blue bars) we compute the difference between the water surface elevation H predicted

NI ET AL. 6 of 17

19447973, 2022, 12, Downloaded

doi/10.1029/2022WR032544 by University Of Washington Lib S, Wiley Online Library on [09/01/2023]. See the Terms

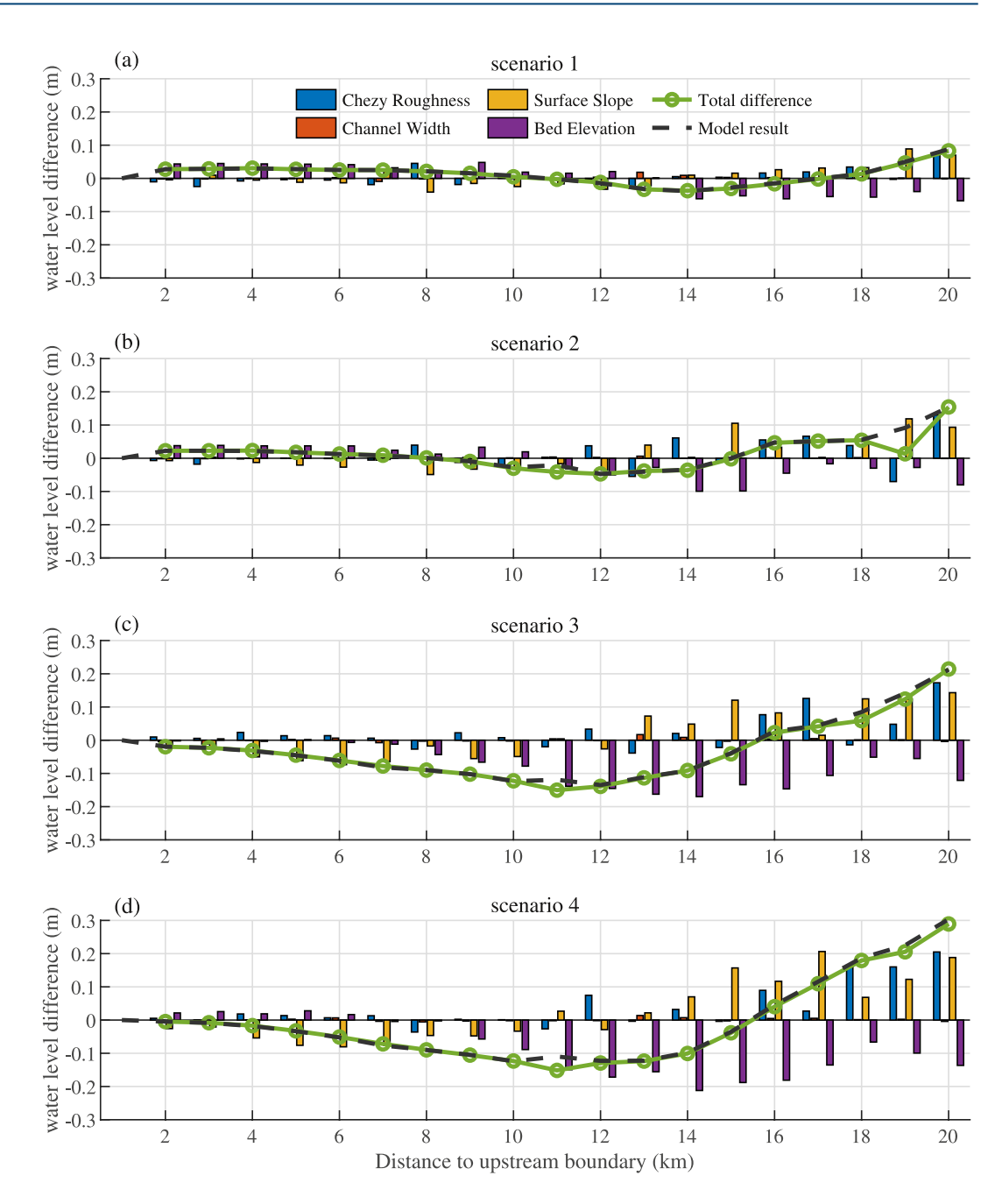


Figure 5. Water level difference relative to base case, including components attributed to bottom roughness, channel width and depth and water surface slope changes according to Chezy formula during peak discharge period of the flood test.

from Equation 2 using model derived parameters from the base case (H(W0,C0,S0,B0)) and the same calculation substituting the value of roughness from scenario 1 (H(W0,C1,S0,B0)).

In all four scenarios, the change in water level relative to the base model during the peak discharge period is concave upward, with the minimum value located in the middle of the estuary, between 11 and 14 km from upstream boundary (Figures 3e, 3h, 3m and 3r). This channel profile is caused primarily by local erosion and results in reduced flood extent in the middle of the estuary in the flood tests. In the lower reaches of the estuary, that is, >14 km from upstream boundary, the channel resistance and the water surface slope both act to increase the water level, overcoming reductions in water level associated with bed erosion. In the upper reach of the estuary, slight sea level rise and severe sea level rise have different effects on the water level. In Scenarios 1 and 2, the increased water levels during peak discharge in the upstream reach is mainly caused by the riverbed elevation

NI ET AL. 7 of 17

19447973, 2022, 12, Downloaded from https://agupubs.onlinelibrary.wiley.com/doi/10.1029/2022WR032544 by University Of Washington Lib S, Wiley Online Library on [09.01/2023]. See the Terms

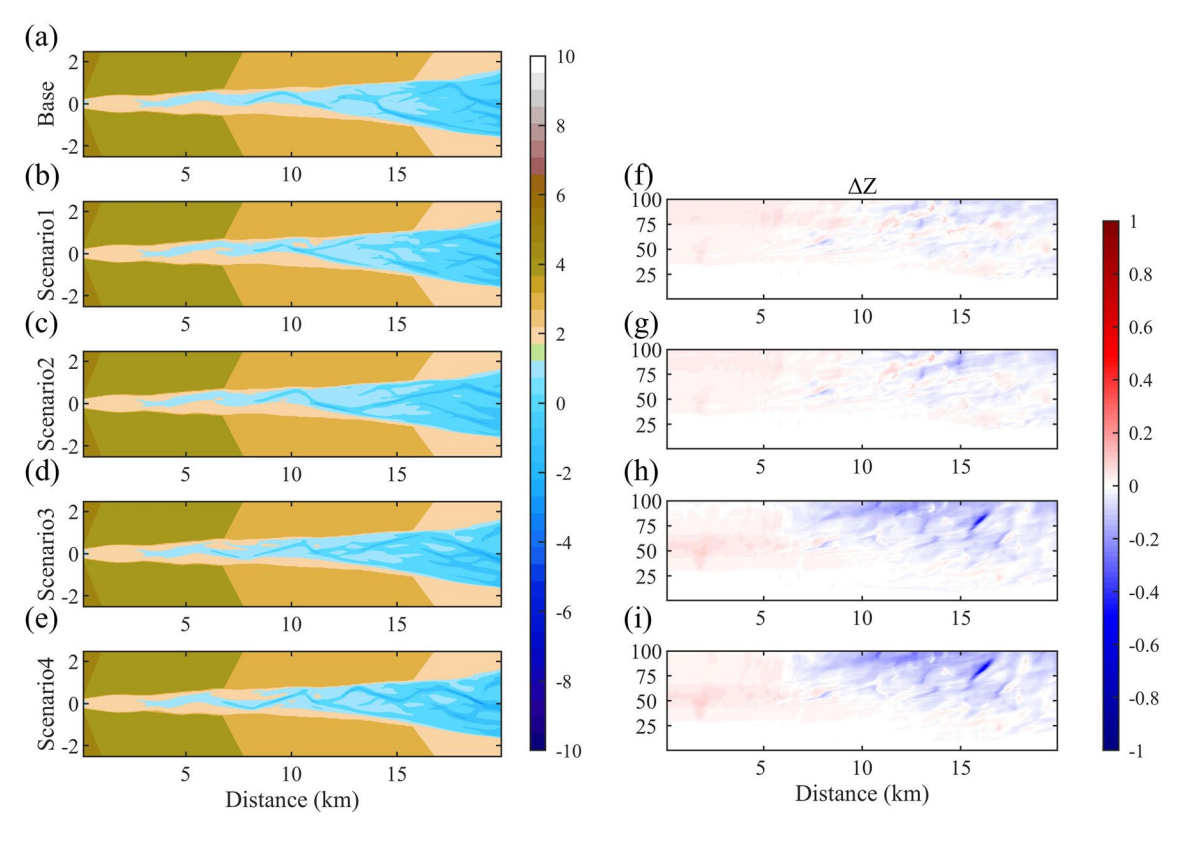


Figure 6. The morphology of at the 100th year considering (a) no SLR, (b) scenario 1, (c) scenario 2, (d) scenario 3 and (e) scenario 4 and cross-channel averaged bed level different between the base model and (f) scenario 1, (g) scenario 2, (h) scenario 3 and (i) scenario 4. Positive values indicate aggradation and negative values indicate erosion compared to the base model.

increase. Scenarios 3 and 4 experience significant water surface decline in the middle of the estuary, leading to an increase in the upstream water surface slope and a decrease in the water surface elevation. These results show that the response of the estuarine system to SLR is sensitive to the interactions between hydrodynamics and morphodynamics and can be significant in reaches far upstream from the river mouth.

# 5. Effects of SLR on Long-Term Estuarine Morphodynamics

A comprehensive understanding of estuarine morphological and hydrological response to SLR is essential in understanding the complexity of estuarine response to SLR during riverine flooding. Figure 6 shows the contour of bed level after the 100-year simulations under different SLR scenarios and the bed level change relative to the base model as a function of longitudinal distance and time for each SLR scenario. We observe that sea-level rise favors deposition in the upstream and erosion in the downstream reaches of the estuary (Figures 6f–6h, 6i). Erosion extends further upstream as SLR increases. In scenario 1 and 2, bed level change at the upstream reaches is constantly increasing until the end (~0.04 m), while in scenario 3 and 4, it reaches its peak value (~0.05 m) around year 60 and then gradually decreases. Comparing the bed elevation evolution with the flood extent evolution (Figure 3), we can see that the bed level trend is consistent with flood extent change. SLR also causes channel width change in these simulations, but the magnitude (~8 m at upstream) and its effect on flood extent change (as in Figure 5) are too small to take into consideration.

Though river discharge remains consistent, mean flow velocity is altered in the presence of SLR as channel morphology and water slope are altered (Figure 7a). With the increase of sea-level, the M2 tidal amplitude and velocity both increase significantly, and the tidal influence extends further upstream until the energy gets dissipated (Figures 7b and 7c). Compared with the no-SLR base case, a SLR of 0.64 m at offshore boundary induces a 0.8 m increase in M2 tidal amplitude and a 0.2 m/s increase in M2 near-bed current velocity at the estuary mouth in scenario 4. The M4 tidal amplitude and near-bed velocity remain stable (about 0.35 and 0.2 m/s) at the estuary

NI ET AL. 8 of 17

19447973, 2022, 12, Downloaded from https://agupubs.onlinelibrary.wiley.com/doi/10.1029/2022WR032544 by University Of Washington Lib S, Wiley Online Library on [09/01/2023]. See the Terms and Condition (https://onlinelibrary.wiley

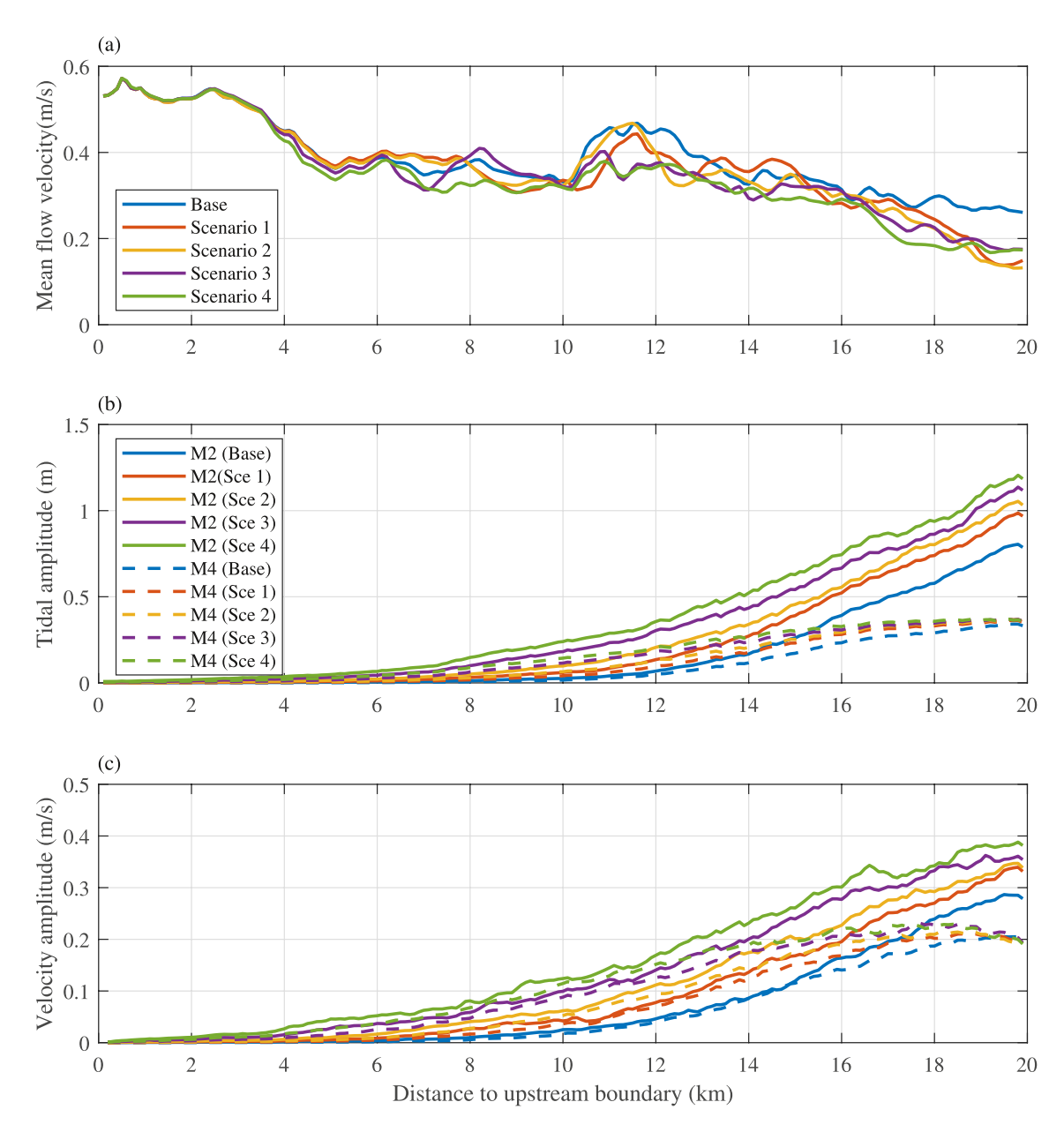


Figure 7. Cross-section averaged Tidal components analysis results at the end of 100 years models. (a): M2 and M4 tide amplitude; (b): M2 and M4 near-bed velocity amplitude; (c): Mean flow velocity.

mouth while the tidal energy dissipation reaches further upstream. Similar results have been presented by Hall et al. (2013), where they find tidal ranges remain constant in the lower part of the estuary but increase by 100% for the upper part of estuary under SLR influence.

Variations in tidal asymmetry are associated with imbalanced flood and ebb tide velocity and duration, and affect residual estuarine sediment transport and trapping capacity. Following Song et al. (2011), the tidal asymmetry parameter  $\gamma$  is calculated as:

$$\gamma = \frac{3}{2} \frac{\alpha_{M_2}^2 \alpha_{M_4} \sin(2\Phi_{M_2} - \Phi_{M_4})}{\left[ \left( \alpha_{M_2}^2 + 4\alpha_{M_4}^2 \right) / 2 \right]^{3/2}} \tag{3}$$

NI ET AL. 9 of 17

19447973, 2022, 12, Downloaded from https://agupubs.onlinelibrary.wiley.com/doi/10.1029/2022WR032544 by University Of Washington Lib S, Wiley Online

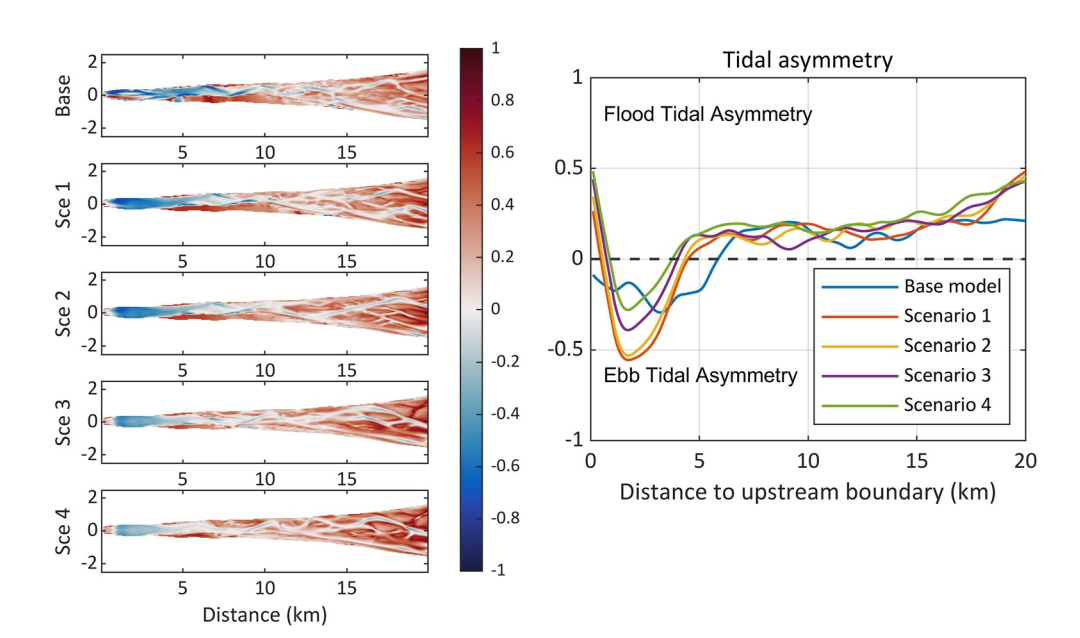


**Figure 8.** Tidal asymmetry parameter  $(\gamma)$  distribution.

where  $\alpha_{M_2}$ ,  $\alpha_{M_4}$  represent the tidal velocity amplitude and  $\Phi_{M_2}$ ,  $\Phi_{M_4}$  represent the tidal phase for M2 and M4 tidal components, respectively. Positive values indicate a tidal asymmetry in flood-tide direction with a longer rising tide and a stronger flood current, while negative values indicate tidal asymmetry in the ebb-tide direction.

In all our tests, an ebb tidal asymmetry is found in subtidal channel areas while intertidal areas are dominated by flood tidal asymmetry (Figure 8), indicating that tidal asymmetry generally favors sea-ward sediment transport in subtidal channels and landward sediment transport in intertidal flats. How tidal component changes induce sediment transport in estuarine area will be further explored in Section 6.

In summary, all four SLR scenarios show common features in tidal response to SLR including suppressed mean flow velocity, increased tidal range, furthermore tidal influence in landward direction, an ebb tidal asymmetry in subtidal channel area and a flood tidal asymmetry on intertidal flats.

# 6. Tidal Residual Sediment Transport

Residual sediment transport in the estuary is under the combined influence of river discharge from upstream and tides from downstream (Van der Molen, 2002). use a simplified transport relationship for tidally averaged sediment transport. The near-bottom instantaneous Eulerian sediment transport vector  $\overrightarrow{Q}_b$  is assumed to be proportional to the third power of the instantaneous near-bottom velocity vector  $\overrightarrow{U}_b$  ( $\overrightarrow{U}_b = \overrightarrow{u} + \overrightarrow{v}$ ):

$$\frac{\overrightarrow{Q_b}}{\alpha} = |U_b|^2 \cdot \overrightarrow{U_b} \tag{4}$$

in which  $\alpha$  is a constant, u and v represent current velocity in along-channel and cross-channel direction, respectively. The result consists of the product of a sediment stirring parameter  $|U_b|^2$  and a sediment carrier parameter  $|U_b|^2$ . The sediment initiation velocity threshold was neglected for simplification. The instantaneous horizontal velocity can be decomposed into the residual flow and two tidal harmonic components (the main harmonic M2 and first overtide M4, higher harmonics are neglected):

$$u = u_0 + u_2 \cos(\omega t - \phi_{2x}) + u_4 \cos(2\omega t - \phi_{4x})$$
 (5)

$$v = v_0 + v_2 \cos(\omega t - \phi_{2y}) + v_4 \cos(2\omega t - \phi_{4y})$$
(6)

NI ET AL. 10 of 17

where  $\omega$  is the frequency of the M2 tidal component;  $\phi$  is the phase of tide velocity component;  $u_0$ ,  $u_2$ ,  $u_4$  and  $v_0$ ,  $v_2$ ,  $v_4$  are the residual flow, M2 tide component and M4 tide component velocity amplitude in along-estuary and cross-estuary direction, respectively; t is time. Substituting Equation 5 and Equation 6 into Equation 4 and applying tidal averaging in longitudinal direction gives:

$$\frac{Q_{x,b}}{\alpha} = Q_{ent} + Q_{eia} + Q_{tia} \tag{7}$$

$$Q_{ent} = u_0 \left( u_0^2 + v_0^2 \right) \tag{8}$$

$$Q_{eia} = u_0 \left[ \frac{1}{2} \left( 3u_2^2 + v_2^2 \right) + \frac{1}{2} \left( 3u_4^2 + v_4^2 \right) \right] + v_0 \left[ u_2 v_2 \cos \left( \phi_{2x} - \phi_{2y} \right) + u_4 v_4 \cos \left( \phi_{4x} - \phi_{4y} \right) \right]$$
(9)

$$Q_{tia} = u_4 \left[ \frac{3}{4} u_2^2 \cos(-\phi_{4x} + 2\phi_{2x}) + \frac{1}{4} v_2^2 \cos(\phi_{4x} - 2\phi_{2y}) \right] + \frac{1}{2} u_2 v_2 v_4 \cos(-\phi_{4y} + \phi_{2x} + \phi_{2y})$$
(10)

in which,  $Q_{x,b}$  represents sediment transport rate in longitudinal direction.  $Q_{ent}$  consisting of only Eulerian residual flow, represents sediment transport due to Eulerian residual flow.  $Q_{eia}$  represents the interactions between the Eulerian residual currents and tidal currents and has the same direction as the Eulerian residual currents.  $Q_{tia}$  is induced by the interaction between the main harmonic M2 tide and its first over-tide M4 tide, reflecting the effect of tide-induced asymmetry. Sediment transport in lateral direction is neglected as its scale is relatively small compared with along-channel direction.

Figure 9 shows the estimation of the residual sediment transport components by Equation (4) based on model results during the last few tidal cycles of the 100 years morphodynamic models.  $Q_{ent}$  and  $Q_{eia}$  are in the seaward direction which correspond to the residual current direction, and  $Q_{tia}$  is in the landward direction. At the upstream part of the domain, residual sediment transport decreases due to suppressed mean flow velocity. In the lower zone, both  $Q_{eia}$  and  $Q_{tia}$  increase and reach further upstream due to higher tidal energy.  $Q_{eia}$  is additionally larger in magnitude, resulting in an increased net seaward sediment transport from 10 to 18 km. This net increase in seaward sediment transport indicates that the increased tidal energy overwhelms the decrease in mean flow velocity and flood-tide asymmetry. It should be noted that due to model limitations, only results of the last few tidal cycles were used for calculation; results in Figure 8 represent only the sediment transport condition at the end of these 100-year simulations.

# 7. Hydrological and Morphological Response to SLR

To investigate how upstream sediment transport is affected by the combined influence of river discharge and tidal components under SLR influence during 100 years, we select the cross-section 5 km from the upstream boundary as a representative location and investigate its morphological evolution. Figure 10 shows the difference in tidally averaged cross-sectionally integrated, sediment flux at the 5 km cross-section for each scenario compared with the base model. At the cross-section 5 km from upstream boundary, SLR favors landward sediment transport before year 60, but after this time, the effect of SLR on sediment transport varies. Over the 100 years of simulation time, water depth, surface slope and Chezy roughness are computed and their effects on mean flow velocity are examined with the classic Chezy formula (Sturm, 2001) (Figure 11). Calculation results (purple line with circles) are generally consistent with model results (gray dashed line). Before year 60, SLR favors landward residual sediment transport in all scenarios (Figure 10) mainly due to altered flow resistance (Figure 11). After year 60, scenario 2 experiences less landward sediment transport than scenario 1 mainly due to changes in water slope. The seaward residual sediment transport in scenarios 3 and 4 also increase significantly after year 60, mainly because of net increases in water surface slope and decreases in flow resistance. However, scenario 4 experiences less total seaward sediment transport in comparison to scenario 3 due to differences in water surface slope. Thus, the residual sediment transport in the estuary channel under SLR is subject to a combined influence of the hydrodynamic response (water slope change) and morphodynmaic response (bed elevation change and bed roughness change).

NI ET AL. 11 of 17

19447973, 2022, 12, Downloaded from https://agupubs.onlinelibrary.wiley.com/doi/10.1029/2022WR032544 by University Of Washington Lib S, Wiley Online Library on [09.01/2023]. See the Terms

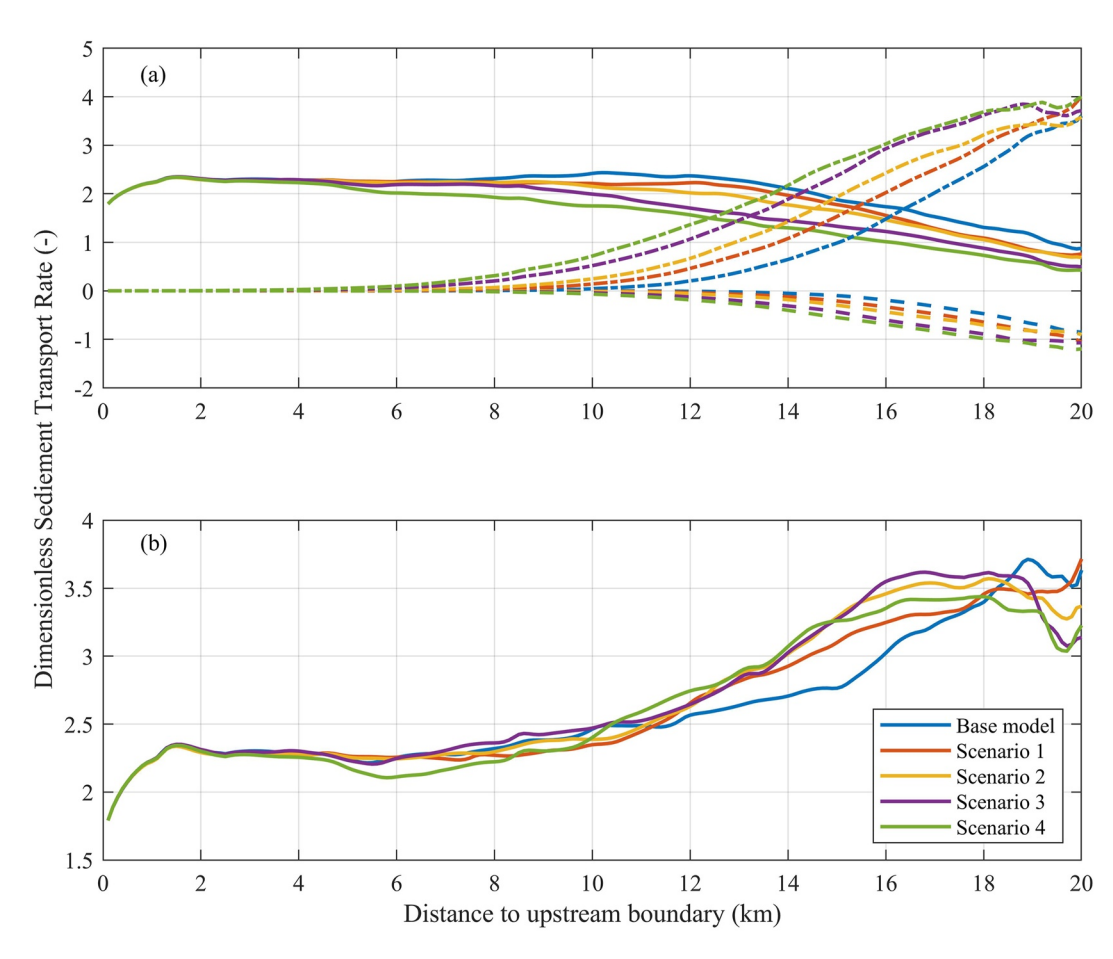


Figure 9. Spatial distribution of dimensionless residual sediment transport with Equations 7–10, (a) Dimensionless residual sediment transport along channel calculated with Sediment proxy:  $Q_{ent}$  (Solid line),  $Q_{eia}$  (Dot-dashed line) and  $Q_{tia}$  (Dashed line), triangles indicate boundary between river-dominant area and transitional zone; (b) Cross-section integrated total dimensionless residual sediment transport rate.

Under a constant upstream sediment supply and water flow, the estuarine morphologic response to SLR is non-linear, resulting primarily from the compound influence of flow resistance and water slope change, as shown in Figures 10 and 11. Our results show that SLR causes significant erosion in downstream sections of the estuary and results in a concave-shaped water level difference along the channel. A similar estuarine morphologic

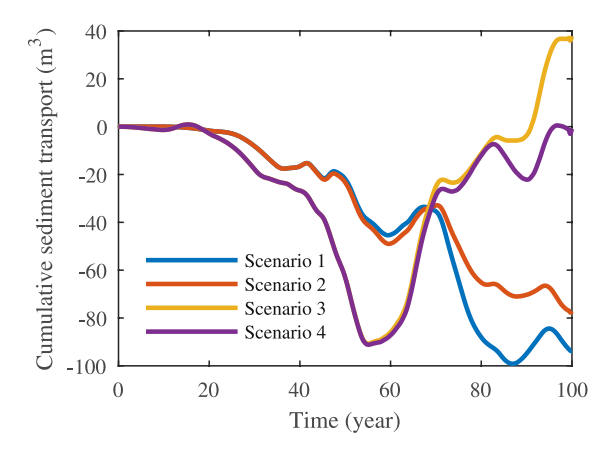


Figure 10. Cumulative sediment transport normalized by the sediment transport in base model at a location 5 km from the upstream boundary.

response to SLR was found by Röbke et al. (2020) in their research on the Western Scheldt estuary, which was based on an 80-year model simulation of a typical funnel-shaped, tidally influenced estuary.

In contrast, Yuan et al. (2020) showed that under SLR influence, the equilibrium channel profile would remain the same shape while the bed level keeps pace with SLR over longer time scales (>4,000 years). Their result suggests that SLR favors sediment trapping along channel in the long-term. Similar results have been found by Ralston et al. (2019), who found that with a long-term sea level rise rate of about 0.3 cm/yr (about the same rate as scenario 2 in our study), SLR could have induced about half of the sediment trapping in the tidal river of Hudson from 1975 to 2015.

Figure 12 illustrates the main hydrodynamic and morphodynamic processes associated with riverine flood extent in channel-estuary systems with SLR impact. SLR has a direct impact on estuarine hydrodynamics and an indirect impact on estuarine morphodynamics. Generally, SLR can amplify tidal energy, increase upstream water slope, decrease downstream water slope and

NI ET AL. 12 of 17

19447973, 2022, 12, Downloaded from https://agupubs.onlinelibrary.wiley.com/doi/10.1029/2022WR032544 by University Of Washington Lib S, Wiley Online Library on [09/01/2023]. See the Terms and Condition (https://onlinelibrary.wiley

nditions) on Wiley Online Library for rules of use; OA articles

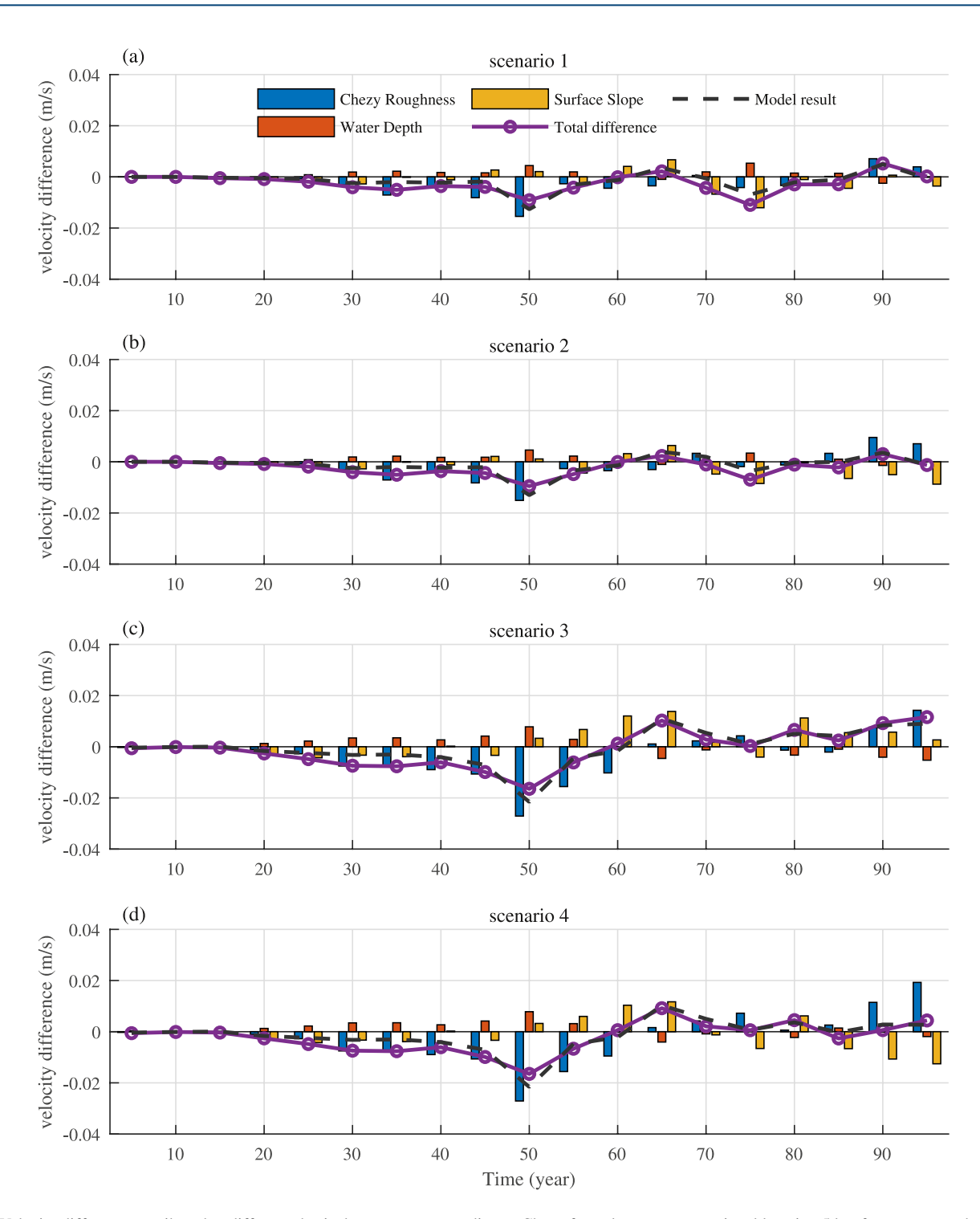


Figure 11. Velocity differences attributed to different physical parameters according to Chezy formula at a cross-sectional location 5 km from upstream boundary. Plotted as a function of time.

decrease residual flow velocity. These hydrodynamic adjustments can occur in days or weeks, while the associated morphodynamic may never reach a new equilibrium with a consistently increasing SLR value applied at the offshore boundary. The existence of the geographic and hydrological feedback loops over various temporal and spatial scales adds to the uncertainty of estuarine response to SLR.

NI ET AL. 13 of 17

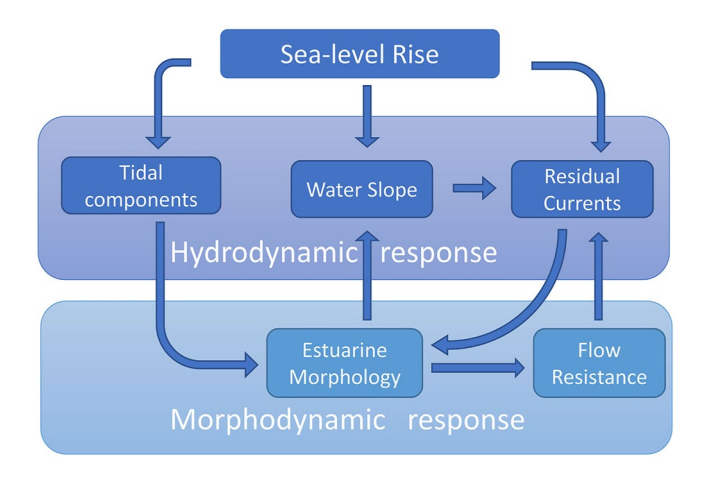


Figure 12. Schematic of geographic and hydrological feedback loops under SLR influence.

The time lag between hydrological and morphological response to SLR becomes important when the observation period is of similar magnitude to the time lag. Wang (1997) found that due to a delayed response between hydrology and morphology, the effect of SLR induced amplified tidal energy on sediment import cannot be observed before about year 30 and it takes longer to compensate its negative effects. In the early stage of SLR influence, an estuary tends to experience more tidal asymmetry in ebb-tide direction, but in the long term, the influence of SLR changes into a flood-tide asymmetry. Kragtwijk et al. (2004) suggested that for a simplified model, morphological evolution of tidal inlets due to a disturbance can be expressed exponentially and the morphological response time can be determined by basin surface area, equilibrium channel volume and sediment concentration etc. However, these explorations mainly focus on the tidal inlets and little research has been done on the morphological evolution of the upstream reaches of estuaries where tidal influence is negligible.

In our study, the cumulative sediment transport in the upstream reach of the system shows a periodic pattern with the sediment transport direction alternating between seaward and landward directed transport compared with the

no SLR case, and their turning points are generally consistent in time (Figure 9). In Figure 10, the most significant transition occurs between the 50th to 65th year, when all four scenarios transition from a weakened seaward flow velocity to a favored one compared with the base case. This change is mainly due to decreased bed roughness and increased water slope and results in a transition from bed deposition to erosion in the upstream domain.

Water slope can be approximated as the superposition of riverbed slope and water depth gradient, and is thus influenced by both morphological and hydrological factors. SLR can decrease the along-channel water slope by increasing the water level offshore. At the same time, SLR can generate a negative bed level gradient in the longitudinal direction and contribute to an increasing water slope. The competition between these two trends determines whether SLR has a positive or negative impact on water surface slope and water level as shown in Figure 5. As hydraulic response is relatively quick and morphologic response is relatively slow, the increasing trend in water slope will only be observed years after the imposed sea level rise, because it lags the morphodynamic adjustment. From the 85th to 100th year water slope changes reduced seaward flow velocity in scenarios 1, 2, and 4 but increased seaward flow velocity in scenario 3. We hypothesize that the hydraulic response in water slope overwhelms the morphological response in scenario 1, 2, and 4 while the opposite is true in scenario 3.

Flow resistance, which is due to grain friction and form roughness, plays an important role in the system response. In our simulations, the resistance law is only used for calculation in the basal layer of cells, whereas the rest of the velocity profile is computed using a logarithmic velocity profile. The constant Chezy roughness we applied in simulations only accounts for the grain friction and small-scale form roughness within the cells. Variations in form roughness are related to channel bathymetry, but are often hard to predict with high accuracy from summary properties of a channel (Ferguson, 2013). We leave it for future research to investigate how flow resistance responds to SLR and how this influences the upstream channel morphodynamic and associated flood extent.

In this study, we were constrained to qualitative assessments of the time lag in morphodynamic response due to limitations in model settings. For example, a non-constant SLR at the offshore boundary made it difficult to determine the actual morphologic response time in a dynamic system. Further exploration of the response time lag between hydrology and morphology is recommended for understanding the channel response to SLR on centurial time scale.

# 8. Limitations and Recommendations for Future Research

For simplification purposes, we consider an idealized funnel-shaped estuary with steady boundary conditions and we neglect many secondary factors that are not relevant for the dominant morphodynamic processes. However, due to the complex interaction between hydrodynamics and bathymetry, a realistic estuary may experience a hydrodynamic and morphological response to SLR that differs from an idealized estuary.

NI ET AL. 14 of 17

It should be noted that this study is not intended to accurately represent the estuarine system in real world. Many important factors have been excluded from the simulation. For example, only single M2 tidal wave has been applied at offshore boundary. Excluding other astronomic constituents affects the non-linear interaction between different tidal components and also estuarine morphology (Parker, 2007). Mutual interactions between predominant (M2 tide) and other astronomic constituent enhance the effetive friction, and a correction of the friction term should be applied to correctly reproduce the correct wave behavior (Cai et al., 2018). The considerations in this study rely on the assumption that upstream discharge and sediment supply were constant. Study shows that extreme flood events have implications for estuary-coastal behavior at the time-scale of several months to decades (Cooper, 2002). At river dominated estuaries, the morphology adjustment of an estuary-coastal system an last for several decades, and tide dominated estuaries can adjust with a faster speed.

Important factors that help to create the unique hydrodynamic regime like wind and ocean wave are also excluded in this study. Ocean wave affects sediment distribution by eroding shorelines, stripping substrates, and redistributing sediments (French et al., 2000; Khojasteh, Glamore, et al., 2021). Wind forcing affects mixing, water levels, flow velocities. The Coriolis effect induced by earth's rotation affects secondary circulations within estuarine system (Xie et al., 2017) and plays an important role in wild estuaries at high latitude (Cossu & Wells, 2013). Excluding these factors from this idealized model helps us focus on the main mechanism that affects long-term morphodynamic evolution.

The effect of SLR on the hydrodynamics of an estuary has been shown to be sensitive to unique aspects of the estuarine geometry such as its morphological evolution and the construction of coastal defenses (Khojasteh, Chen, et al., 2021). Du et al. (2018) pointed out the importance of estuary length in tidal response to SLR. Tidal amplitude is likely to decrease in short estuaries but increase in long estuaries. Leuven et al. (2019) found that estuarine shape and size significantly influence their hydrodynamic responses to SLR. Also, simulations that capture inland inundation experience a decrease in tidal amplitude toward the coast due to a change in the magnitude and spatial distribution of tidal energy and resonance effects (Carless et al., 2016; Pelling & Green, 2014). Similar results have been presented by Lee et al. (2017), who show that without the existence of levees, the tidal range decreases due to increased energy dissipation in newly inundated areas. It should be noted that the coastal flood in our test is weak, due to the fact that the bank height we applied at the shoreline was higher than the high tide water level. Study also found that restricted entrances in estuaries increase the tidal velocity in the restricted zone but decrease in the upstream reach, and could offset SLR induced tidal range amplification (Khojasteh et al., 2020).

Moreover, vegetation and human activities like channel dredging and land reclamation are not considered. Vegetation tends to increase channel bed roughness and increase bed resilience (Kirwan et al., 2016), and human activities constrain local morphodynamic evolution. These factors are excluded from our simulation, but may significantly change tidal propagation and morphological adaptation in a realistic estuary under SLR. The idealized model simulates a small channel-estuary system under a mesotidal condition and uses the Skagit River as a prototype, but it is not an exact representation of a natural tidal basin. Thus, applications of findings from this idealized model should be limited to the morphology and external forcings in this study.

# 9. Conclusion

This study analyzes the morphodynamic and riverine flood extent of an idealized estuary under different SLR scenarios over the next century. Sea-level rise scenarios projected by Miller et al. (2018) are imposed at the offshore boundary of an idealized model based on the Skagit River to simulate five different scenarios including a base case with no SLR. The model results demonstrate that changes in riverine flood extent occur as a result of the combined influence of changes in local bed level, water slope, and flow resistance. Under severe SLR conditions, due to the amplification of tidal energy, the estuary experiences an increase in seaward sediment transport, while the upstream tends to deposit. A concave-upward shaped water level difference along the channel increases the upstream water slope. Moreover, upstream deposition is weakened or even turns into erosion due to altered water slope and flow resistance. These hydrological (increased water surface slope) and morphological (weakened upstream deposition) factors together decrease riverine flood extent in the upstream reaches over the next century under high SLR conditions.

NI ET AL. 15 of 17

19447973, 2022, 12, Downloaded from

# **Data Availability Statement**

Delft3D software used in this study is an open-source software. Source code and software package can be downloaded via <a href="https://svn.oss.deltares.nl/repos/delft3d/trunk">https://svn.oss.deltares.nl/repos/delft3d/trunk</a>. Software version of 7545 was used in this study. Registration and license file need to be applied. A Matlab formatted result data and a plot script used in this study can be downloaded via <a href="https://doi.org/10.7910/DVN/7GMTTL">https://doi.org/10.7910/DVN/7GMTTL</a>.

#### Acknowledgments

Wuming Ni's visit to the University of Washington is sponsored by China Scholarship Council (CSC NO.201806320313). The authors are grateful for funding from the NSF PREEVENTS program (Award 1663859) and NSF Cascadia CoPes Hub (Award 213713). This work was facilitated through the use of advanced computational, storage, and networking infrastructure provided by the Hyak supercomputer system and funded by the STF at the University of Washington. We are grateful for Nirnimesh Kumar's help and inspiration with his work. He was a friend and we miss him dearly.

# References

- Ahrendt, S., Horner-Devine, A. R., Collins, B. D., Morgan, J. A., & Istanbulluoglu, E. (2022). Channel conveyance variability can influence flood risk as much as streamflow variability in western Washington state. *Water Resources Research*, 58(6), e2021WR031890. https://doi.org/10.1029/2021wr031890
- Bilskie, M., Hagen, S., Medeiros, S., & Passeri, D. (2014). Dynamics of sea level rise and coastal flooding on a changing landscape. *Geophysical Research Letters*, 41(3), 927–934. https://doi.org/10.1002/2013gl058759
- Braat, L., Van Kessel, T., Leuven, J. R., & Kleinhans, M. G. (2017). Effects of mud supply on large-scale estuary morphology and development over centuries to millennia. *Earth Surface Dynamics*, 5(4), 617–652. https://doi.org/10.5194/esurf-5-617-2017
- Cai, H., Savenije, H., & Toffolon, M. (2014). Linking the river to the estuary: Influence of river discharge on tidal damping. *Hydrology and Earth System Sciences*, 18(1), 287–304. https://doi.org/10.5194/hess-18-287-2014
- Cai, H., Toffolon, M., Savenije, H. H., Yang, Q., & Garel, E. (2018). Frictional interactions between tidal constituents in tide-dominated estuaries. Ocean Science, 14(4), 769–782. https://doi.org/10.5194/os-14-769-2018
- Canestrelli, A., Lanzoni, S., & Fagherazzi, S. (2014). One-dimensional numerical modeling of the long-term morphodynamic evolution of a tidally-dominated estuary: The lower fly river (Papua New Guinea). Sedimentary Geology, 301, 107–119. https://doi.org/10.1016/j.sedgeo.2013.06.009
- Carless, S. J., Green, J. M., Pelling, H. E., & Wilmes, S.-B. (2016). Effects of future sea-level rise on tidal processes on the patagonian shelf. *Journal of Marine Systems*, 163, 113–124. https://doi.org/10.1016/j.jmarsys.2016.07.007
- Cooper, J. (2002). The role of extreme floods in estuary-coastal behaviour: Contrasts between river-and tide-dominated microtidal estuaries. Sedimentary Geology, 150(1–2), 123–137. https://doi.org/10.1016/s0037-0738(01)00271-8
- Cossu, R., & Wells, M. G. (2013). The evolution of submarine channels under the influence of coriolis forces: Experimental observations of flow structures. *Terra Nova*, 25(1), 65–71. https://doi.org/10.1111/ter.12006
- Curran, C. A., Grossman, E. E., Mastin, M. C., & Huffman, R. L. (2016). Sediment load and distribution in the lower skagit river, skagit county, Washington (Tech. Rep.). US Geological Survey.
- Czuba, J. A., Magirl, C. S., Czuba, C. R., Grossman, E. E., Curran, C. A., Gendaszek, A. S., & Dinicola, R. S. (2011). Sediment load from major rivers into puget sound and its adjacent waters. US Department of the Interior, US Geological Survey.
- Du, J., Shen, J., Zhang, Y. J., Ye, F., Liu, Z., Wang, Z., et al. (2018). Tidal response to sea-level rise in different types of estuaries: The importance of length, bathymetry, and geometry. *Geophysical Research Letters*, 45(1), 227–235. https://doi.org/10.1002/2017gl075963
- Elmilady, H. M., Van der Wegen, M., Roelvink, D. J., & Van der Spek, A. (2020). Morphodynamic response of intertidal shoals to sea level rise. Agu fall meeting abstracts, 2020, OS009–0010.
- Engelund, F., & Hansen, E. (1967). A monograph on sediment transport in alluvial streams. Technical University of Denmark 0stervoldgade (Vol. 10).
- Ferguson, R. (2013). 9.5 reach-scale flow resistance. In J. F. Shroder (Ed.), Treatise on geomorphology (pp. 50–68). Academic Press. https://doi.org/10.1016/b978-0-12-374739-6.00230-x
- French, C. E., French, J. R., Clifford, N. J., & Watson, C. J. (2000). Sedimentation–erosion dynamics of abandoned reclamations: The role of waves and tides. Continental Shelf Research, 20(12–13), 1711–1733. https://doi.org/10.1016/s0278-4343(00)00044-3
- Guo, L., Van der Wegen, M., Roelvink, J., & He, Q. (2014). The role of river flow and tidal asymmetry on 1-d estuarine morphodynamics. *Journal of Geophysical Research: Earth Surface*, 119(11), 2315–2334. https://doi.org/10.1002/2014jf003110
- Gutierrez, B. T., Plant, N. G., & Thieler, E. R. (2011). A bayesian network to predict coastal vulnerability to sea level rise. *Journal of Geophysical Research*, 116(F2). https://doi.org/10.1029/2010jf001891
- Hall, G. F., Hill, D. F., Horton, B. P., Engelhart, S. E., & Peltier, W. (2013). A high-resolution study of tides in the delaware bay: Past conditions and future scenarios. *Geophysical Research Letters*, 40(2), 338–342. https://doi.org/10.1029/2012gl054675
- Hamman, J. J. (2012). Effects of projected twenty-first century sea level rise, storm surge, and river flooding on water levels in puget sound floodplains and estuaries. University of Washington.
- Hamman, J. J., Hamlet, A. F., Lee, S.-Y., Fuller, R., & Grossman, E. E. (2016). Combined effects of projected sea level rise, storm surge, and peak river flows on water levels in the skagit floodplain. *Northwest Science*, 90(1), 57–78. https://doi.org/10.3955/046.090.0106
- Hong, B., Liu, Z., Shen, J., Wu, H., Gong, W., Xu, H., & Wang, D. (2020). Potential physical impacts of sea-level rise on the pearl river estuary, China. *Journal of Marine Systems*, 201, 103245. https://doi.org/10.1016/j.jmarsys.2019.103245
- Khojasteh, D., Chen, S., Felder, S., Heimhuber, V., & Glamore, W. (2021). Estuarine tidal range dynamics under rising sea levels. *PLoS One*, 16(9), e0257538. https://doi.org/10.1371/journal.pone.0257538
- Khojasteh, D., Glamore, W., Heimhuber, V., & Felder, S. (2021). Sea level rise impacts on estuarine dynamics: A review. Science of The Total Environment, 780, 146470. https://doi.org/10.1016/j.scitotenv.2021.146470
- Khojasteh, D., Glamore, W., Heimhuber, V., Hottinger, S., & Felder, S. (2019). Implications of tidal resonance and water depth on predicting sea level rise in estuaries. *Australasia Coasts & Ports*. 10–13.
- Khojasteh, D., Hottinger, S., Felder, S., De Cesare, G., Heimhuber, V., Hanslow, D. J., & Glamore, W. (2020). Estuarine tidal response to sea level rise: The significance of entrance restriction. *Estuarine, Coastal and Shelf Science*, 244, 106941. https://doi.org/10.1016/j.ecss.2020.106941
- Kirwan, M. L., Temmerman, S., Skeehan, E. E., Guntenspergen, G. R., & Fagherazzi, S. (2016). Overestimation of marsh vulnerability to sea level rise. *Nature Climate Change*, 6(3), 253–260. https://doi.org/10.1038/nclimate2909
- Koch, F., & Flokstra, C. (1980). Bed level computations for curved alluvial channels: Prepared for the 19th iahr congress, new Delhi, India, February 1981. Waterloopkundig Laboratorium.
- Kragtwijk, N., Zitman, T., Stive, M., & Wang, Z. (2004). Morphological response of tidal basins to human interventions. *Coastal Engineering*, 51(3), 207–221. https://doi.org/10.1016/j.coastaleng.2003.12.008

NI ET AL. 16 of 17

- Lane, S., Tayefi, V., Reid, S., Yu, D., & Hardy, R. (2007). Interactions between sediment delivery, channel change, climate change and flood risk in a temperate upland environment. Earth Surface Processes and Landforms: The Journal of the British Geomorphological Research Group, 32(3), 429–446. https://doi.org/10.1002/esp.1404
- Lane, S., & Thorne, C. (2007). River processes. Future flooding and coastal erosion risks. Thomas Telford, 82–99. https://doi.org/10.1680/ffacer.34495.0006
- Lanzoni, S., & Seminara, G. (2002). Long-term evolution and morphodynamic equilibrium of tidal channels. *Journal of Geophysical Research*, 107(C1), 1. https://doi.org/10.1029/2000jc000468
- Le Bars, D., Drijfhout, S., & De Vries, H. (2017). A high-end sea level rise probabilistic projection including rapid Antarctic ice sheet mass loss. Environmental Research Letters, 12(4), 044013. https://doi.org/10.1088/1748-9326/aa6512
- Lee, S. B., Li, M., & Zhang, F. (2017). Impact of sea level rise on tidal range in chesapeake and delaware bays. *Journal of Geophysical Research: Oceans*, 122(5), 3917–3938. https://doi.org/10.1002/2016jc012597
- Lesser, G. R., Roelvink, J. V., Van Kester, J. T. M., & Stelling, G. (2004). Development and validation of a three-dimensional morphological model. Coastal Engineering, 51(8–9), 883–915. https://doi.org/10.1016/j.coastaleng.2004.07.014
- Leuven, J. R., Pierik, H. J., Vegt, M. v. d., Bouma, T. J., & Kleinhans, M. G. (2019). Sea-level-rise-induced threats depend on the size of tide-influenced estuaries worldwide. *Nature Climate Change*, 9(12), 986–992. https://doi.org/10.1038/s41558-019-0608-4
- Miller, I. M., Morgan, H., Mauger, G., Newton, T., Weldon, R., Schmidt, D., et al. (2018). Projected sea level rise for Washington state: A 2018 assessment.
- Mockus, V. (1957). Use of storm and watershed characteristics in synthetic hydrograph analysis and application. US Dept. of Agriculture, Soil Conservation Service.
- Moore, R. D., Wolf, J., Souza, A. J., & Flint, S. S. (2009). Morphological evolution of the dee estuary, eastern Irish sea, UK: A tidal asymmetry approach. *Geomorphology*, 103(4), 588–596. https://doi.org/10.1016/j.geomorph.2008.08.003
- Morgan, J. A., Kumar, N., Horner-Devine, A. R., Ahrendt, S., Istanbullouglu, E., & Bandaragoda, C. (2020). The use of a morphological acceleration factor in the simulation of large-scale fluvial morphodynamics. *Geomorphology*, 356, 107088. https://doi.org/10.1016/j.geomorph.2020.107088
- Mulamba, T., Bacopoulos, P., Kubatko, E. J., & Pinto, G. F. (2019). Sea-level rise impacts on longitudinal salinity for a low-gradient estuarine system. Climatic Change, 152(3), 533–550. https://doi.org/10.1007/s10584-019-02369-x
- Olabarrieta, M., Geyer, W. R., Coco, G., Friedrichs, C. T., & Cao, Z. (2018). Effects of density-driven flows on the long-term morphodynamic evolution of funnel-shaped estuaries. *Journal of Geophysical Research: Earth Surface*, 123(11), 2901–2924. https://doi.org/10.1029/2017jf004527 Parker, B. B. (2007). Tidal analysis and prediction.
- Partheniades, E. (1965). Erosion and deposition of cohesive soils. *Journal of the Hydraulics Division*, 91(1), 105–139. https://doi.org/10.1061/jvceai.0001165
- Passeri, D. L., Hagen, S. C., Plant, N. G., Bilskie, M. V., Medeiros, S. C., & Alizad, K. (2016). Tidal hydrodynamics under future sea level rise and coastal morphology in the northern gulf of Mexico. Earth's Future, 4(5), 159–176. https://doi.org/10.1002/2015ef000332
- Pelling, H. E., & Green, J. M. (2014). Impact of flood defences and sea-level rise on the European shelf tidal regime. *Continental Shelf Research*, 85, 96–105. https://doi.org/10.1016/j.csr.2014.04.011
- Prandle, D. (2009). Estuaries: Dynamics, mixing, sedimentation and morphology. Cambridge University Press.
- Ralston, D. K., Talke, S., Geyer, W. R., Al-Zubaidi, H. A., & Sommerfield, C. K. (2019). Bigger tides, less flooding: Effects of dredging on barotropic dynamics in a highly modified estuary. *Journal of Geophysical Research: Oceans*, 124(1), 196–211. https://doi.org/10.1029/2018jc014313
- Röbke, B. R., Elmilady, H., Van Der Wegen, M., & Taal, M. (2020). The long-term morphological response to sea level rise and different sediment strategies in the western scheldt estuary (The Netherlands) (Tech. Rep.). Deltares.
- Roelvink, J. (2006). Coastal morphodynamic evolution techniques. Coastal Engineering, 53(2–3), 277–287. https://doi.org/10.1016/j.coastaleng.2005.10.015
- Slater, L. J., Singer, M. B., & Kirchner, J. W. (2015). Hydrologic versus geomorphic drivers of trends in flood hazard. *Geophysical Research Letters*, 42(2), 370–376. https://doi.org/10.1002/2014gl062482
- Song, D., Wang, X. H., Kiss, A. E., & Bao, X. (2011). The contribution to tidal asymmetry by different combinations of tidal constituents. *Journal of Geophysical Research*, 116(C12). https://doi.org/10.1029/2011jc007270
- Stover, S., & Montgomery, D. (2001). Channel change and flooding, skokomish river, Washington. *Journal of Hydrology*, 243(3–4), 272–286. https://doi.org/10.1016/s0022-1694(00)00421-2
- Sturm, T. W. (2001). Open channel hydraulics (International Edition ed.). McGraw-Hill Higher Education.
- Van der Molen, J. (2002). The influence of tides, wind and waves on the net sand transport in the north sea. Continental Shelf Research, 22(18–19), 2739–2762. https://doi.org/10.1016/s0278-4343(02)00124-3
- Van der Wegen, M., Dastgheib, A., & Roelvink, J. (2010). Morphodynamic modeling of tidal channel evolution in comparison to empirical pa relationship. Coastal Engineering, 57(9), 827–837. https://doi.org/10.1016/j.coastaleng.2010.04.003
- Van Rijn, L. C. (2011). Analytical and numerical analysis of tides and salinities in estuaries; part i: Tidal wave propagation in convergent estuaries. Ocean Dynamics, 61(11), 1719–1741. https://doi.org/10.1007/s10236-011-0453-0
- Vu, D., Yamada, T., & Ishidaira, H. (2018). Assessing the impact of sea level rise due to climate change on seawater intrusion in mekong delta, vietnam. Water Science and Technology, 77(6), 1632–1639. https://doi.org/10.2166/wst.2018.038
- Wang, Z. (1997). Morfologische interactie westerschelde estuarium en het mondingsgebied: Asmita-westerschelde: Een gedragsgeoriënteerde modellering (tech. Rep.). Deltares (WL).
- Xie, D., Gao, S., Wang, Z. B., Pan, C., Wu, X., & Wang, Q. (2017). Morphodynamic modeling of a large inside sandbar and its dextral morphology in a convergent estuary: Qiantang estuary, China. *Journal of Geophysical Research: Earth Surface*, 122(8), 1553–1572. https://doi.org/10.1002/2017jf004293
- Yang, Z., & Khangaonkar, T. (2009). Modeling tidal circulation and stratification in skagit river estuary using an unstructured grid ocean model. Ocean Modelling, 28(1–3), 34–49. https://doi.org/10.1016/j.ocemod.2008.07.004
- Yu, Q., Wang, Y., Gao, S., & Flemming, B. (2012). Modeling the formation of a sand bar within a large funnel-shaped, tide-dominated estuary: Qiantangjiang estuary, China. *Marine Geology*, 299, 63–76. https://doi.org/10.1016/j.margeo.2011.12.008
- Yuan, B., Sun, J., Lin, B., & Zhang, F. (2020). Long-term morphodynamics of a large estuary subject to decreasing sediment supply and sea level rise. Global and Planetary Change, 191, 103212.

NI ET AL. 17 of 17